Electronic Supplementary Material (ESI) for Journal of Materials Chemistry A.

Bottom-up synthetic hierarchical buffer structure of copper silicon nanowire hybrids as ultra-stable and high-rate lithium-ion battery anodes

Hucheng Song[1], Sheng Wang[1], Xiaoying Song[1], Huafeng Yang[1], Gaohui Du[2], Linwei Yu[1], Jun Xu[1], Ping He*[1], Haoshen Zhou*[1,3], Kunji Chen[1]*

[1]National Laboratory of Solid State Microstructures and Collaborative Innovation Center of Advanced Microstructures/School of Electronics Science and Engineering and Center of Energy Storage Materials & Technology College of Engineering and Applied Sciences, Nanjing University, Nanjing 210093, China

[2]Institute of Physical Chemistry, Zhejiang Normal University, Jinhua 321004, China

[3]Energy Technology Research Institute National Institute of Advanced Industrial Science and Technology (AIST) Umezono 1-1-1, Tsukuba 3058568, Japan

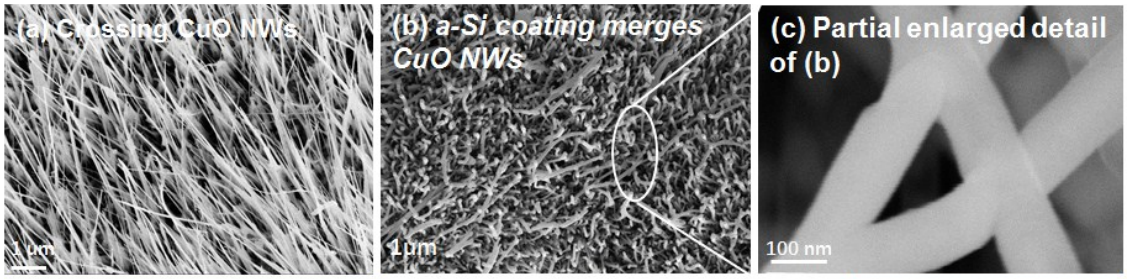

Figure S1. (a) SEM image of the crossing CuO NWs. (b), (c) Low- and high-magnification SEM of interconnected CuO/a-Si core-shell NWs after coating an amorphous silicon layer.

The SEM image of as-prepared CuO NWs has demonstrated a large and high-density matrix of crisscrossing CuO NWs that measure approximately 5-10 μm long and 40-50 nm wide in the middle diameter (see in Fig. S1a). After coating a uniform amorphous silicon upon the crisscrossing CuO NWs by PECVD technique, a highly interconnected CuO/a-Si core-shell nanowire structure is obtained with a varying thickness averaging 40 nm, as shown in the partially enlarged detail of Fig. S1c. It is interesting to note that the amorphous silicon-coated layer could act as a glue layer to weld the crossing CuO NWs together,

forming a three-dimensional continuous and interconnected core-shell nanowire network (see Fig. S1b and S1c).

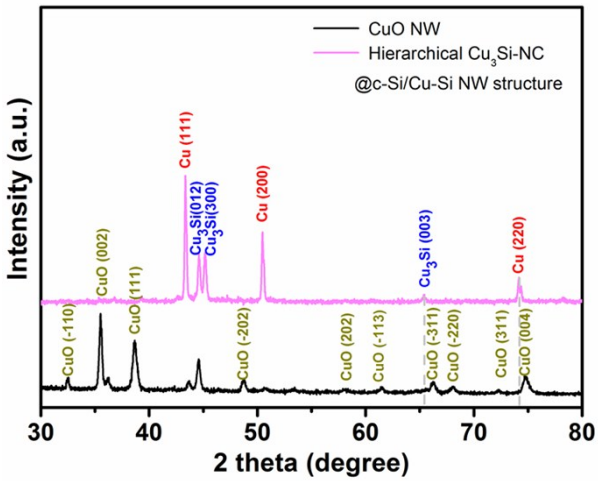

Figure S2. XRD analysis of CuO NW structure grown on copper oxide foam and hierarchical Cu-Si NW hybrid structure grown on the whole copper foam.

According to the X-ray diffraction (XRD) analysis shown in Figure S2, a high-temperature H_2 annealing at 480°C has been sufficient to activate the alloy-forming process of copper silicon, leading to the disappear of all diffraction peaks belonged to CuO (002), (111), (004) and (-110) crystalline planes, located at 35.5°, 38.7°, 74.8° and 32.5°, respectively. The now strongest diffraction peaks emerge at 43.4°, 50.5° and 74.3° which correspond to the crystalline planes of Cu (111), (200) and (220). Meanwhile, two addition peaks emerge at 44.5° and 44.9° corresponding to the two strongest diffraction peaks of Cu_3Si. This indicates that the CuO cores can be completely'' reduced to Cu that then continues to diffuse and alloy with silicon (including both the a-Si outer shell layer and the c-Si NWs branch) during the high-temperature H_2 annealing process. The total amount of silicon is acquired through weighing the total mass of the sample before and after loading silicon.

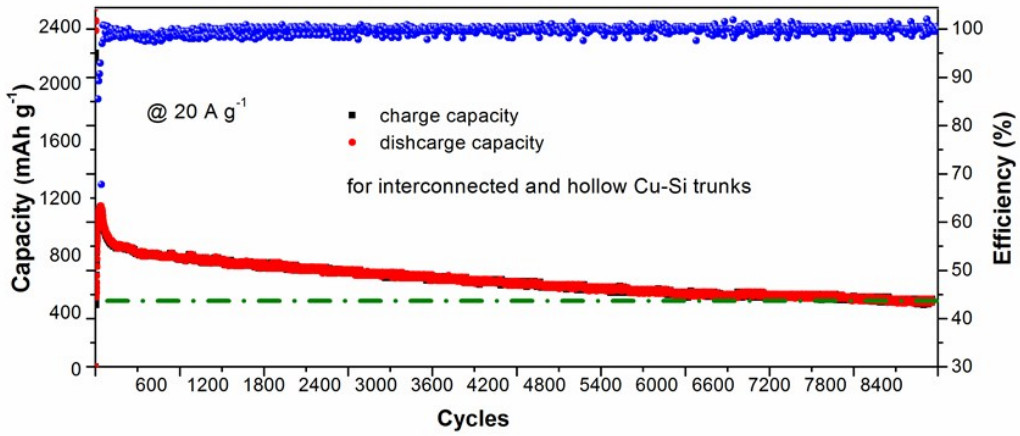

Figure S3. Ultra-long term-cycling performance for interconnected and hollow Cu-Si trunks at 20 A g^{-1}.

Figure S3 shows the ultra-stable cycle performance of this interconnected and hollow Cu–Si trunks at a current density of 20 A g^{-1} with 9000 cycles. The increasing discharge capacity from the initial 500 mAh g^{-1} to 1100 mAh g^{-1} of 80th cycle can be observed. This rise in capacity indicates a typical activation process of the Si nanomaterial at a high current density where the silicon storage medium becomes only partially lithiated over the initial cycles [29, 30]. Excluding the initial activation process, a retention rate is defined as the ratio of the final capacity to that obtained at the 800th cycle, to be ≈of 60% after 9000 cycles. This implicates indeed an Ultra-long cycle lifespan and ultrafast charging operation, as inferred from Figure S3 that allows a cycle lifespan of 9000 cycles and a full battery charging process in ≈3 min with yet two times higher capacity than that of graphite LIBs (372 mAh g^{-1}).

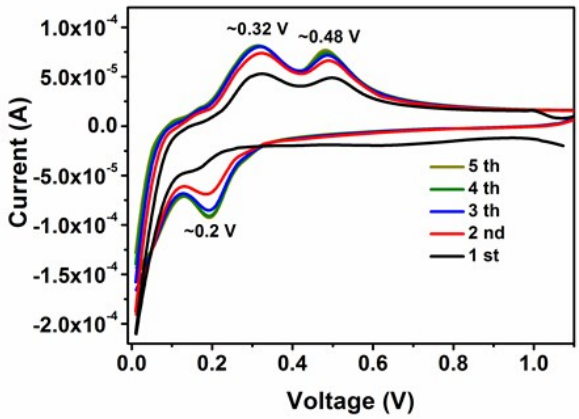

Figure S4. Cyclic voltammetry curves for the first five cycles of hierarchical Cu-Si NW hybrid structure at a scan rate of 0.0001 V s^{-1} with the voltage range of 0.01–1.1 V.

Figure S4 shows the current–voltage curves of a LIB with hierarchical Cu_3Si-QD@c-Si/Cu-Si NW anode, where a large discharging current surge below 0.2 V can be assigned to the Li-ion insertions into the a-Si matrix and the crystallization process of a-$Li_{15}Si_4$. In the reverse charging scan, the two oxidation current peaks at around 0.3 and 0.5 V correspond to the delithiation process of Li_xSi back to a-Si. These discharge/charge voltages have been reported in Si-based anode materials [3, 29, 30].

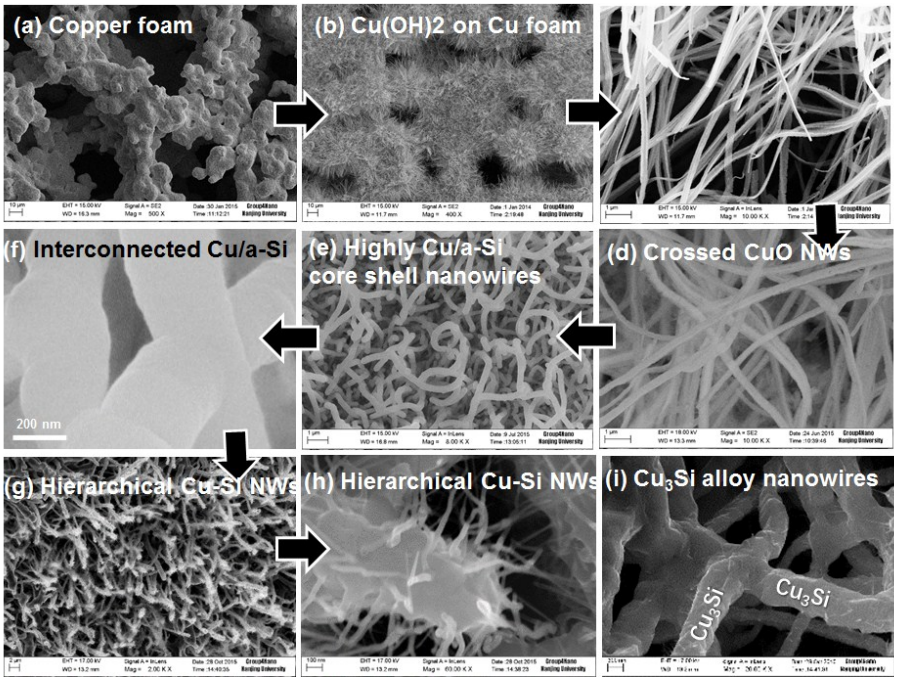

Figure S5. Morphology and structure characterization of hierarchical Cu_3Si NWs. (a) The SEM images of the copper foam substrate. (b), (c) Low and high-magnification SEM of the as-grown $Cu(OH)_2$ NWs. (d) Crossing CuO NWs. (d) the crossing CuO NWs after calcination; (e) the interconnected Cu/a-Si core–shell nanowires after coating an a-Si layer and a low-temperature H_2 annealing, with an enlarged view presented in (f). (g) Hierarchical Cu_3Si NWs after grafting Si NWs and a high-temperature H_2 annealing at 600 ^oC for 8 h, while (i) and (h) provide close views of the trunks and branches.

Figure S5 (a)–(f) show the SEM images of the Cu foam substrate, the as-grown $Cu(OH)_2$ NWs, the CuO NWs and the CuO/a-Si core–shell, respectively. As we can see in Figure S5 (b), with an enlarged view provided in S5(c), the random $Cu(OH)_2$ NWs grown over the rough Cu foam substrate are mutually crossing with a length of about 30 to 50 μm. After calcination at 350 °C for 3 h, the dehydrated CuO NWs are found to become more flexible with a slightly bending morphology, as seen in Figure S5(d). With a subsequent a-Si layer coating and a low temperature H_2 annealing, the diameter of the interconnected Cu/a-Si core–shell increases to about ~500 nm, as shown in Figure S5(e) and (f). After that, Si NW branches are grown mediated via a Sn-droplet-catalyzed VLS growth upon the interconnected Cu/a-Si core shell NW trunks, when the substrate temperature is raised to 560 °C and a mixture gas of 5 sccm SiH_4 and 50 sccm H_2 was introduced, with chamber pressure of 600 mTorr and RF power of 76 mW/cm^2 for 60 min. Finally, the hierarchical Cu_3Si NWs has been obtained after a high-temperature H_2 atmosphere annealing of 600 °C for 8 h, as shown in Figure S5 (g)–(i), which could accelerate the diffusion of Cu into silicon medium to obtain.

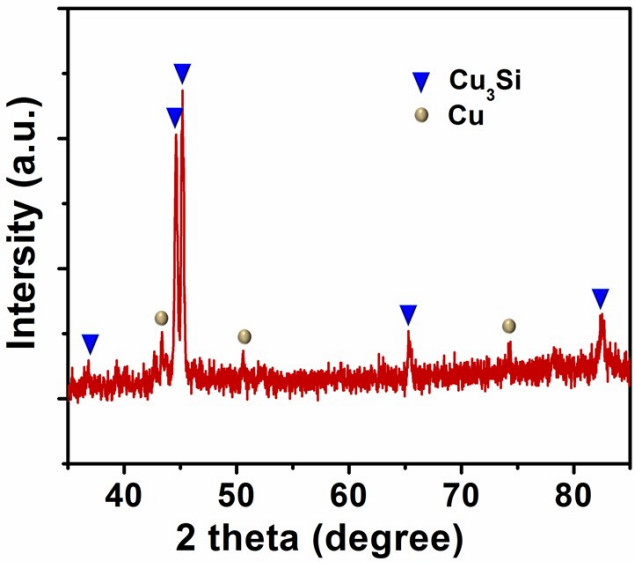

Figure S6. XRD analysis of hierarchical Cu_3Si NWs.

According to the X-ray diffraction analysis as shown in Figure S6, after a high-temperature H_2 reduction at 600 °C for 8 h, the four strongest diffraction peaks positioned at 44.5°, 44.9°, 65.4° and 82.5° all come from the diffraction crystalline planes of Cu_3Si. Meanwhile, another three

weak diffraction peaks form Cu foam substrate have been also observed. These results indicate a thorough conversion process of Cu to Cu_3Si.

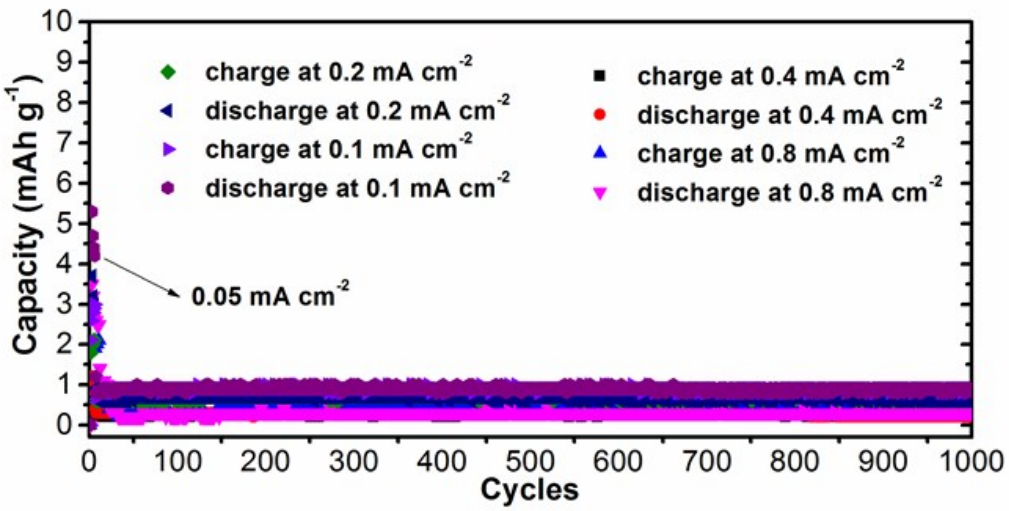

Figure S7. Cycling performance for hierarchical Cu_3Si NWs at 0.1 mA cm^{-2}, 0.2 mA cm^{-2}, 0.4 mA cm^{-2}, and 0.8 mA cm^{-2} respectively.

Figure S7 shows the cycling performance of the hierarchical Cu_3Si NWs. The mass loading of hierarchical Cu_3Si NWs increases to 5.0 mg cm^{-2}–10.0 mg cm^{-2}. A relatively low current density of 0.05 mA cm^{-2} has first been applied to stabilize the SEI film and activate the storage medium during the initial 5 cycles. The extremely low initial discharge/charge capacities of less than 6 mAh cm^{-2} have been demonstrated in the hierarchical Cu_3Si NWs anode even at a Si mass loading such mass loading up to 10 mg cm^{-2}. After initial five cycles, all specific capacities of Cu_3Si NWs are less than 1 mAh cm^{-2} at 0.1 mA cm^{-2}, 0.2 mA cm^{-2}, 0.4 mA cm^{-2}, and 0.8 mA cm^{-2} respectively. That indicated that Cu_3Si is a Li-inactive alloy material during the discharge/charge cycle process.

Table 1: A summary of the performances of different Si-loaded nanoparticles, nanowires, nanotubes and its complex structures from the 2nd to the last cycle in the literature, [3,10,13,26,30,32, 42-54] in comparison to what is achieved in this work.

Material & structure	Mass load [mg cm^{-2}]	Current density [A g^{-1}]	Cycle lifespan [cycles]	Capacity after cycles [mAh g^{-1}]	Capacity retention	Areal Capacity [mAh cm^{-2}]	Ref.

Si NW array Grown on SS	0.5	1/20 C	10	≈3120	≈73%	1.5	[3]
c-Si@a-Si Core-shell NW array	0.2	0.85	100	≈1060	≈85%	0.2	[43]
Cu-Si-Al_2O_3 Nanocable array	----	1.4 0.3-70-0.3	100 60	≈1560 ≈200	≈90% ≈76%	----	[32]
Cu-Si core shell Nanotube array	0.3	0.84 1.3-50-1.3	400 50	≈1500 ≈410	≈60% ≈97%	0.4 0.1	[30]
Interconnected Si NW array	1.2	8.4 0.4-34-0.4	72 70	≈1800 ≈420	≈84% ≈84%	2.2 0.5	[44]
Si/CNT Coaxial nanofiber	0.74	0.2	100	≈1700	≈83%	1.3	[45]
a-Si@CNF core-shell NW array	1.6	0.5	55	≈1900	≈80%	3.0	[46]
c-Si NW/CNT Composite structure	1.8	0.4	65	≈600	≈78%	1.1	[42]
c-Si/SnO_2 NW Hierarchical structure	1.5	0.36	100	≈1200	≈68%	1.8	[10]
c-Si/Ge NW Heterostructures structure	----	C/2	100	≈1256	≈95%	----	[47]
Double-walled Si nanotube	0.03	50 4.2-84-4.4	6000 700	≈600 ≈550	≈88% ≈85%	0.2 ----	[13]
hierarchically Si nanoparticles	2.3 g cm^{-3}	1.8	600	≈1200	≈90%	0.5	[48]
Si sponge structure	0.5	0.1-1.0	1000	≈640	≈81%	1.5	[49]
MSC-Si/G Nanohybrids on Cu foam	1.0	0.2	100	≈1500	----	1.5	[50]
Si/C pomegranate structure	0.2	2.1	1000	≈1160	≈97%	3.0	[26]
Si-nanolayer-embedded graphite	1.6 g cm^{-3}	C/2	100	≈517	≈92%	3.3	[51]
Branch-trunk Si anode embedded with Cu_3Si quantum dots	**1.3** ---	3.0 3.2-12.8-3.2	800 260	≈830 ≈500	≈84% ≈100%	3.5 ----	this work
where the interconnected and hollow Cu-Si trunks	0.3	20	6000	≈560	≈70%	----	this work